

# Boundary dynamics in competing critical black hole formation

Cole Kelson-Packer\* and John Belz†

*Department of Physics and Astronomy,  
University of Utah  
Salt Lake City, Utah 84112,  
USA*

(Dated: October 22, 2021)

Expanding upon our previous study of competing critical phenomena in black hole formation, we numerically investigate the behavior of the dominant perturbative mode across the boundary separating asymptotically dispersing and collapsing regions in a two-dimensional phase space of initial data. We find that across the Type II section of the boundary the mode remains constant, equal to the reciprocal of Choptuik’s well-known quasi-universal exponent, while across the Type I section the mode appreciably varies. We postulate that this change reflects the existence of a third critical solution in addition to the two primary competing attractors, whose dominant perturbative mode is close to that of the Type I critical solution.

## I. INTRODUCTION

Throughout its scholarly history, the study of black holes in General Relativity has yielded a wealth of strange and wondrous results providing key insights into the behavior of classical gravity in the strongly interacting regime. One of the cornerstones of numerical investigations into black holes is the existence of critical phenomena accompanying their formation (M.W. Choptuik, 1993). Generically, it has been found that when some parameter (e.g. amplitude) associated with matter sources in the initial data is varied, there exists a threshold between black hole formation and asymptotic dispersal (D. Christodoulou, 1986a,b, 1987). Time evolutions of initial data near this threshold exhibit various quasi-universal phenomena (M.W. Choptuik, 1993), such as mass power laws with quasi-universal exponents, echoing effects, or predictable scaling in the time-to-collapse of the lapse (C. Gundlach, 2007, 2003). In our previous paper (C. Kelson-Packer and J. Belz, 2020), we encountered, over the course of several hundreds of simulations, the apparently counterintuitive effects of multicritical collapse, whereby two near-critical fields appear to frustrate, rather than accentuate, black hole formation.

The starting point for our investigation was the idea that some kind of interesting interaction should be observed between near-critical massive and massless scalar fields. Since the massive scalar field exhibits Type I and Type II criticality in different regions of the parameter space of initial data (P.R. Brady, C.M. Chambers, and S.M.C.V. Gonçalves, 1997), it might be reasonably hypothesized that such configurations are especially susceptible to Type II perturbations in the Type I phase. We

observed that the two fields, when both are tuned near criticality, appear to inhibit each other’s collapsing tendencies, and suggested that this result may be attributed to the existence of a third critical solution, similar to a scenario proposed by Gundlach et al. (C. Gundlach, T.W. Baumgarte, and D. Hilditch, 2019).

We reprint here for convenience the picture representing the primary results of our previous paper and review its significance. Figure 1 depicts a kind of phase diagram with respect to initial amplitudes for a massless and a massive scalar field minimally coupled to gravity. Each marker represents the result of a numerical simulation taken at reasonable precision and resolution. Marker color reflects the black hole formation mass given its coordinate initial amplitudes, with the darkest red indicating asymptotic dispersal. Marker shape, meanwhile, presents a somewhat crude classification of the dominant critical mechanism preceding collapse, which can reasonably be determined by the time-to-collapse of the lapse variable. The dark horizontal and vertical lines denote the critical amplitudes past which black holes will form if one of the fields were taken alone. The fact that dispersal scenarios exist at larger amplitudes even past the intersection of these lines suggests that the two fields have a mutually inhibiting effect on each other. This is a nonintuitive effect: what is in a naive sense a greater concentration of mass-energy has the result of interfering – rather than augmenting – collapse.

In our previous work we suggested that a rough dynamical systems explanation suffices to explain our results. The essential idea is that the earlier critical evolution of the massless field in a sense draws the the spacetime away from the critical surface corresponding to the massive field that would otherwise be dispositive of asymptotic behavior. A simple interpretation might reduce this to a physically-motivated triviality, corresponding to an exchange of energy between the two fields, wherein the

\* u0980902@utah.edu

† belz@physics.utah.edu

massless field implodes through the origin, carrying away some of the energy of the massive field. What is significant is that this loose physical argument could just as well be turned the other way: that is, the concentration of the massive field about the origin could be suspected to focus and retain the massless field. The dynamical systems picture, however, suggests that the (locally in time) dominant growing mode dictates the actual course of evolution, implicating the frustration we observed. It also explains why the dispersal region impinges so considerably across the Type I critical vertical line – yet barely across the Type II critical horizontal line – in Fig 1.

The purpose of this paper is to more rigorously quantify the dynamical mechanisms at work so as to further justify the assertions made in our previous paper, as well as explain other phenomena we have since observed. We further justify the classifications depicted in Fig. 1, showing how very different perturbative modes are pre-dominant across different parts of the collapse/dispersal boundary. We also discuss how an observed change in the value of the dominant mode along the Type I section of the boundary supports the existence of a third critical solution at the triple point, in addition to reflecting complexities that render part of the Type I section of the boundary numerically intractable.

## II. METHODS

The methods employed in our numerical simulations are the same standard techniques (T.W. Baumgarte and S.L. Shapiro, 2010; M. Alcubierre, 2008; W.H. Press, S.A. Teukolsky, W.T. Vetterling, and B.P. Flannery, 2007) as those adumbrated in our previous paper (C. Kelson-Packer and J. Belz, 2020). We summarize our methodology as follows: we take the standard ADM decomposition assuming spherical symmetry and work in the polar areal gauge. The matter content (massless and massive scalar fields) is evolved in time using fourth-order Runge-Kutta according to the equations

$$\begin{aligned} \partial_t \Phi_i &= \frac{\alpha}{a} \Pi_i, & i &= 1, 2, \\ \partial_t \Psi_i &= \partial_r \left( \frac{\alpha}{a} \Pi_i \right), & i &= 1, 2, \\ \partial_t \Pi_i &= \frac{1}{r^2} \partial_r \left( \frac{\alpha r^2}{a} \Psi_i \right) - \alpha a m_i^2 \Phi_i, & i &= 1, 2, \\ m_2 &= 0. \end{aligned} \quad (1)$$

with simple Sommerfeld boundary conditions imposed at large  $r$ , and appropriate anti-/symmetry constraints enforced across the staggered origin. Meanwhile, the metric equations are solved on each full time step (extrapolated during intermediate steps) following

$$\partial_r a = \frac{a}{2} \left[ \frac{1-a^2}{r} + \frac{r}{2} \sum_{i=1}^2 (\Pi_i^2 + \Psi_i^2) + \frac{m_1^2 r}{2} a^2 \Phi_1^2 \right], \quad (2)$$

$$\partial_r \alpha = \alpha \left[ \frac{\partial_r a}{a} + \frac{a^2 - 1}{r} - \frac{m_1^2 r}{2} a^2 \Phi_1^2 \right], \quad (3)$$

subject to the boundary conditions of  $a$  being unity at the origin and  $\alpha$  taken asymptotically Schwarzschild-like. Finally, convergence is checked against the momentum constraint

$$0 = M \equiv \alpha \frac{r}{2} (\Pi_1 \Psi_1 + \Pi_2 \Psi_2) - \partial_t a, \quad (4)$$

which validates our code pursuant to the standards of typical convergence tests, showing it to be fourth-order accurate as designed.

This paper employs standard methods for numerically examining dynamical systems (A. Stuart and A.R. Humphries, 1998; S. Strogatz, 2015; G. Teschl, 2012). Near criticality, we expect that nondimensionalized functions  $Z_p(x, t)$  can be expanded as

$$Z_p(x, t) \approx Z^*(x, t) + C(x) * (p - p^*) * e^{\gamma t} + \dots, \quad (5)$$

where  $Z^*$  denotes the function  $Z_p$  when the tuning parameter  $p$  is at criticality  $p^*$ ,  $\gamma$  is the most dominant growing mode, and  $t$  is a time variable appropriate to the critical system (C. Gundlach, 2007, 2003). In this paper, we consistently take  $p$  to be the amplitude of an initial spherically-symmetric gaussian shell, while we variably take  $Z$  to be  $\Phi$ ,  $r\Pi$ , or  $r\Psi$ . The specific choice is purely aesthetic, in that for all simulations performed each choice lends itself to the same essential results and conclusions.

We perform this analysis by taking the difference of two data sets very close to criticality, taking the  $L^2$  norm of this difference, and then conducting an appropriate regression to obtain an estimate for  $\gamma$ . Explicitly, we take the difference of Eq 5 for two distinct values of  $p$ :

$$Z_{p_1}(x, t) - Z_{p_2}(x, t) \approx C(x) * (p_1 - p_2) * e^{\gamma t} + \dots, \quad (6)$$

of which we then take the  $L^2$  norm to remove spatial dependence, resulting in an approximation taking the form

$$y(t) \approx C(p_1 - p_2) * e^{\gamma t} + \dots, \quad (7)$$

which is in a form readily subjected to regression analysis.

This regression is typically valid for a reasonable time interval near collapse, which we determine by monitoring when  $\alpha$  drops beneath  $10^{-7}$ , or when NaN errors arise from the substantial curvature developing at the origin. It is important that the data for this linearization be taken from a reasonable time interval: if the data comes from too close to collapse, higher order terms become relevant, while if it's taken too long before, other modes significantly contribute. Given also that fine-structure undulations inevitably feature in these regressions as well,

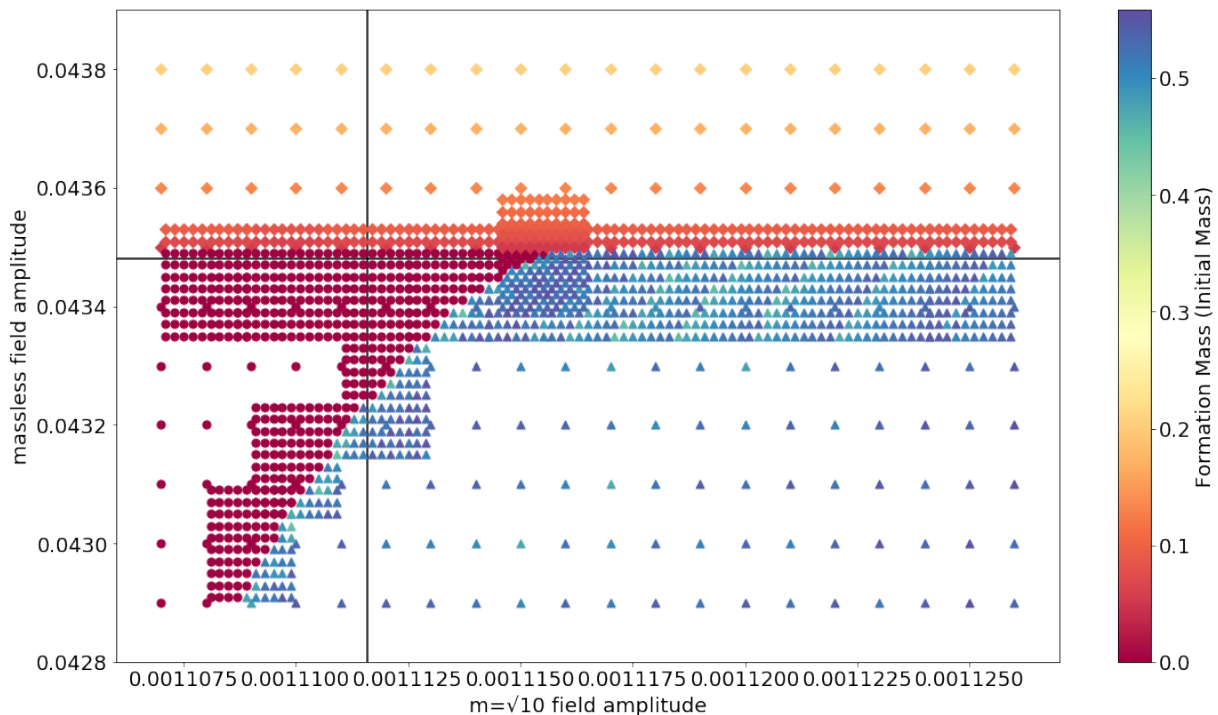


**FIG. 1:** Phase diagram of time evolution behavior for the multicritical field configuration considered in this paper and its predecessor. The axis variables correspond to the amplitudes tuning the initial data of the scalar fields that ultimately determine whether the time evolution of that data collapses or disperses. The circles indicate dispersal, the triangles denote Type I collapse, and the diamonds are Type II collapse – this is determined by the asymptotic time-to-collapse of the lapse, or the failure so to. The color scale is a measure of the mass of the black hole formed. If the initial data evolves to be asymptotically dispersing, this is set to zero mass. We repeat the observation that the above picture suggests the presence of a mechanism that qualitatively inhibits black hole formation.

conducting these regressions is something closer to an art than a rigorous science, which is to say that the margins of error for the derived modes are greater than the ones suggested by the regressions alone.

The validity of these perturbative regression estimates can be checked against other observable quantities dependent upon the dominant mode  $\gamma$  and the tuning parameter  $p$ 's deviation from its critical value  $p^*$ . For Type II collapse, we may compare with a regression on a local measure of black hole initial formation mass near criticality (C. Gundlach, 1997):

$$M \approx A(p - p^*)^{1/\gamma}, \quad (8)$$

where, for our purposes, we will be ignoring the well-known fine-structure corrections (S. Hod and T. Piran, 1996), although their undulations are readily observed in the results *infra*. Meanwhile, for Type I collapse, we carry out a cross-check with the collapse time:

$$T_{\text{collapse}} \approx \text{const.} - \frac{1}{\gamma} \log(|p - p^*|). \quad (9)$$

Solving for and perturbing the exact solution in the style of, say, (C. Gundlach, 1995) would provide much more precise values of the dominant mode  $\gamma$ . However,

this would not seem so feasible for our scenario, which admits features that preclude both the single-variable self-similarity of the Type II exact solution (C. Gundlach, 1997), as well as the metastable soliton star style appropriate to the Type I exact solution (P.R. Brady, C.M. Chambers, and S.M.C.V. Goncalves, 1997; E. Seidel and W. M. Suen, 1990a,b). We obtain in any case sufficiently adequate agreement between the perturbation analysis and the observable quantity analysis to make this greater precision unnecessary for the results we report and our analysis thereof.

### III. RESULTS

#### A. Type II Boundary

We find that the massive field does not significantly affect the fundamental dynamics of Type II criticality. Specifically, we find that the presence of a massive scalar field does not alter the dominant mode associated with the Choptuon in the limit of the pure massless field.

Table I and Fig 2 illustrate our point. Each entry in Table I reflects a log-log regression of black hole formation mass versus the massless field amplitude's deviation

from criticality, while each panel in Fig. 2 depicts a perturbative regression analysis via a log-log regression of the  $L^2$  difference between two simulations near criticality versus logarithmic time-to-collapse. Figure 3 depicts all the mass regressions together for ready comparison by eye.

The same value of the dominant mode,  $\gamma \approx 2.66$ , is observed within reasonable precision across the board. This is the same as the reciprocal of the critical exponent as that associated with the case of the pure massless field investigated by Choptuik (M.W. Choptuik, 1993). Accordingly, the presence of the massive field has only a quantitative effect on evolutionary dynamics near criticality. It does not qualitatively alter the fundamental mechanisms near collapse as reflected in the dominant mode  $\gamma$ , though naturally the secondary field continues to fall in after the lapse collapses and contributes to the developing black hole mass.

Type II Collapse Mass Regressions			
Massive Field Amplitude	Slope	Intercept	Dominant Mode ( $\gamma$ )
0.0	0.373	0.248	2.68
0.0006	0.378	0.308	2.64
0.0008	0.378	0.317	2.65
0.001	0.376	0.322	2.66
0.0011156	0.373	0.269	2.68

**TABLE I:** Linear regression analyses performed on the masses of black holes formed along the Type II section of the collapse/dispersal boundary. Each table entry represents data taken with the amplitude of the massive field fixed, while the massless field’s amplitude varies. All values for  $\gamma$  are found to agree well with that of the pure massless scalar field

## B. Type I Boundary

In contrast to the Type II section of the boundary, the presence of a second field has a significant effect upon Type I collapse. This manifests in the behavior of the dominant mode associated to the Type I critical solution, which in fact varies depending upon the massless field amplitude.

Table II and Fig 4 communicate this point similarly to their Type II counterparts. Each entry in Table II reflects a log-log regression taken for the asymptotic time-to-collapse versus the massive field amplitude’s deviation from criticality, while the panels collected in Fig. 4 show various perturbative analyses performed via log-log regressions of the  $L^2$  difference between two simulations near criticality versus time-to-collapse. Fig 5 compiles all the time-to-collapse regressions to better facilitate comparison by eye.

We observe that, in contrast to the Type II case, the value of the dominant mode  $\gamma$  noticeably changes. Near the triple point, it takes on the value  $\gamma \approx 0.34$ . However, near the regime of a pure massive field,  $\gamma$  takes on a value closer to  $\approx 0.27$ . Moreover, we note a significant decrease in the typical time-to-collapse as we near the triple point. This second fact matches the intuition that frustrated multicriticality otherwise runs against: collapse still happens “earlier,” as we might expect due to the presence of extra matter in the form of the secondary field, despite the counterintuitive inhibition of collapse seen in the shift in criticality.

Some entries and sets in in Table II and Fig 4 are labelled by additional suffixes. This is because, as shown in Fig 6, distinct and numerically consistent ridges appear in some collapse-of-the-lapse regressions. Even moderately away from the triple point, apparent jumps in the time-to-collapse are observed along the Type I section of the boundary. Whether these jumps completely disappear or not near the triple point has not been determined.

Type I Collapse Time Regressions			
Massless Field Amplitude	Slope	Intercept	Dominant Mode ( $\gamma$ )
0.0 (I)	-3.72	198.	0.269
0.0 (II)	-3.72	451.	0.269
0.04 (I)	-3.10	66.9	0.322
0.04 (II)	-3.56	160.	0.281
0.043	-2.90	66.8	0.345
0.0434	-2.88	65.8	0.347

**TABLE II:** Linear regressions performed on times-to-collapse of the lapse for black holes forming along the Type I section of the collapse/dispersal boundary. Each entry represents data taken with the amplitude of the massless field fixed, while the massive field’s varies.  $\gamma$  appears to take on a different value depending on whether the massless field amplitude places the scenario near triple point, or whether it’s near the pure massive field case, and may vary across different ridges of linearity appearing in the data.

While the two most prominent slopes in the left panel of Fig 6 appear to be equal, the two slopes in the panel on the right slightly differ. This variance appears to not be numerical error, as it is reflected in the perturbative analysis in Fig 9. The top plot of Fig 9 depicts a sort of rotation of the right panel of Fig 6. The evolution of the perturbation passes through distinct regimes, with different dominant slopes modulated by underlying undulations. The two intervals of greatest growth are depicted in the lower two plots of Fig 9. The dominant modes obtained therefrom appreciably match those derived from the individual ridges of the right panel of Fig 6, which

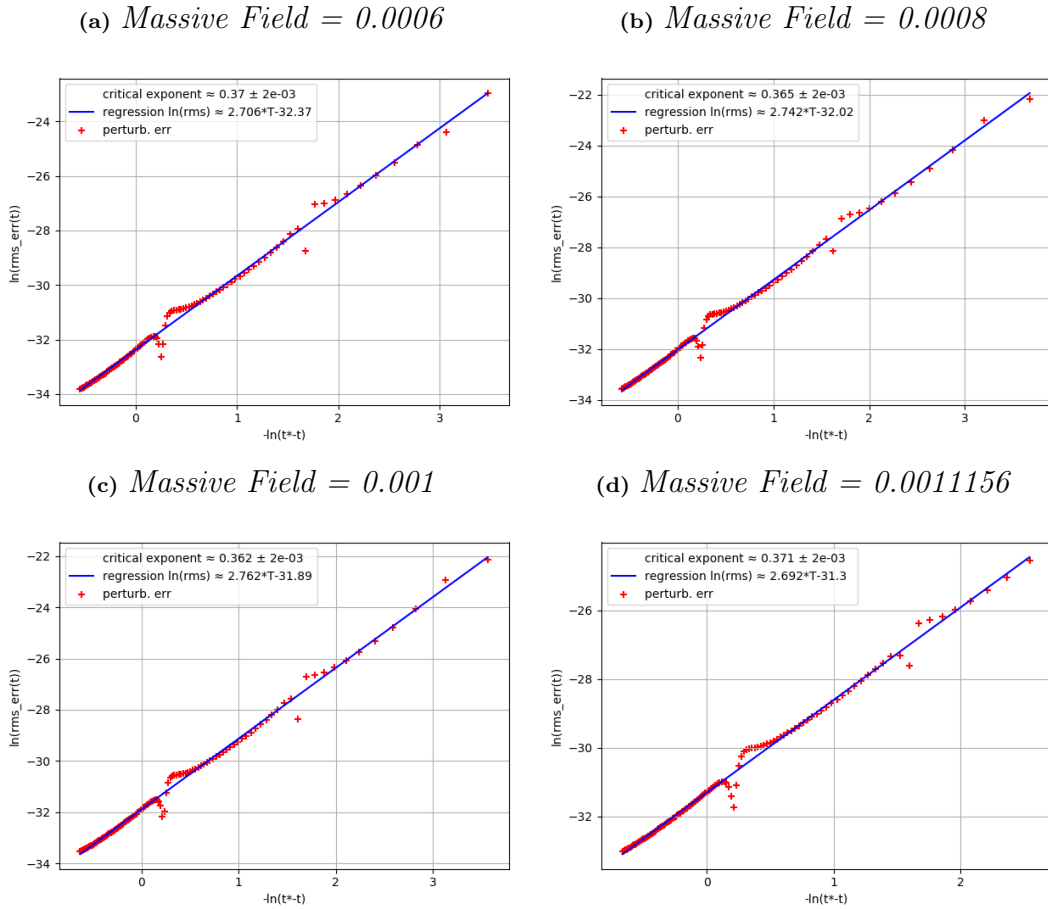


**FIG. 2:** Perturbative analyses performed on pairs of near-critical data arising from simulations near the Type II section of the collapse/dispersal boundary. Each panel represents data taken with the amplitude of the massive field fixed, while the massless field’s varies. The values for  $\gamma$  reasonably match their counterparts in Table I, validating our results.

are depicted in detail in Fig 8, covering ordinate intervals roughly commensurate with the abscissa intervals of their counterparts. The two apparent dominant modes have approximate values 0.32 and 0.28

The equivalent contrasting story expanding upon the left panel of Fig 6 is present in Figs 10 and Fig 7. In this case, as previously said, the slopes are approximately equal, tending around 0.26.

#### IV. DISCUSSION

In our previous paper, we postulated that the multi-critical phenomena seen in our scenario could reflect an alternative dynamical situation considered by Gundlach et al. (C. Gundlach, T.W. Baumgarte, and D. Hilditch, 2019), which they ultimately dismissed in the case they considered. This possibility is illustrated in Fig 11 here, which shares a kinship with Fig 13 of their paper. Between the two primary attractors at play (the Choptuon and the family of metastable soliton stars) there exists a third critical solution influencing the dynamics with its

own dominant perturbative mode. Our results *supra*, featuring an apparently changing dominant mode along the Type I section of the boundary, support this conclusion: the “competition” we observe in our setup would appear to feature, as it were, a third belligerent.

Another comparison with Gundlach et al.’s paper is apposite to our point. In Fig 8 of their paper, they observe “breaks” in the apparent critical exponent for their scenario in the region of their phase space where the Yang-Mills field mostly – but not overwhelmingly – dominates the scalar field. They ascribe these breaks to a straightforward change between their two critical solutions, moving from the massless critical solution ( $\gamma \approx 0.37$ ) to the Yang-Mills critical solution ( $\gamma \approx 0.2$ ). It might be wondered if the “jumps” we observe are similar in nature.

We do not construe the evidence such that our results can be attributed so. The dominant mode along the Type II section of the collapse/dispersal boundary is  $\approx 2.7$ , derived from a logarithmic time scale. Meanwhile, the two differing dominant modes observed along the Type I section of the boundary appear to range around

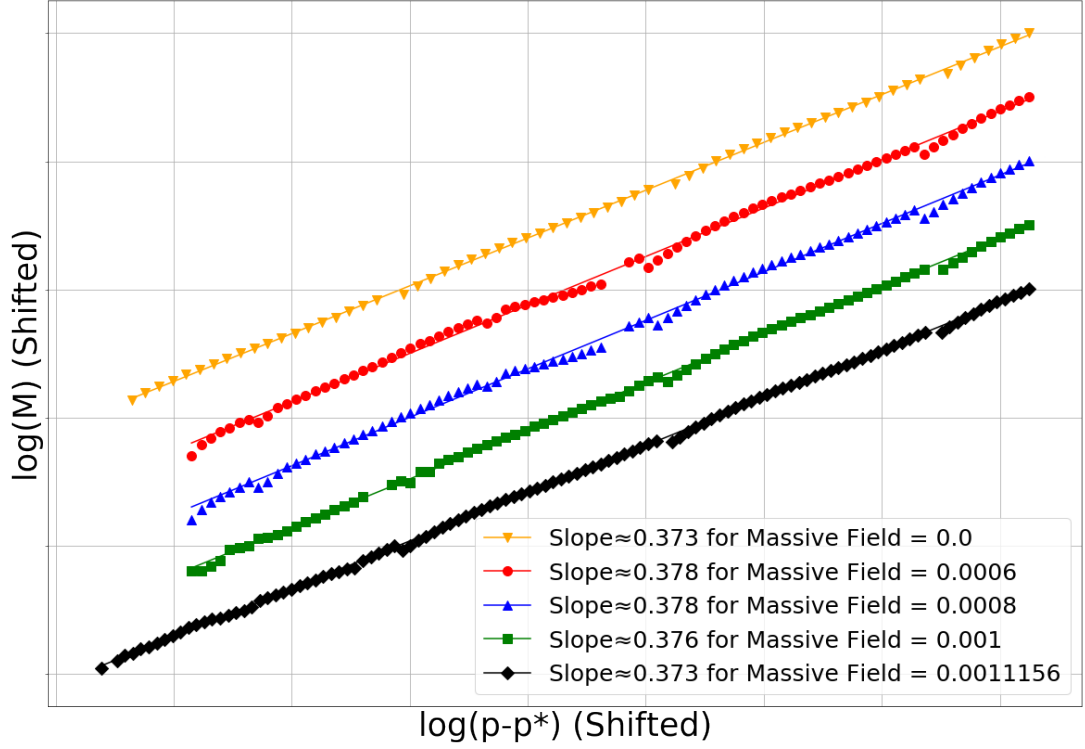


**FIG. 3:** A compilation of the linear regression analyses performed on the masses of black holes formed near the Type II section of the dispersal/collapse boundary. Each set of points cocolored has been shifted uniformly, keeping the slope intact, so as to better present all slopes for comparison by eye.

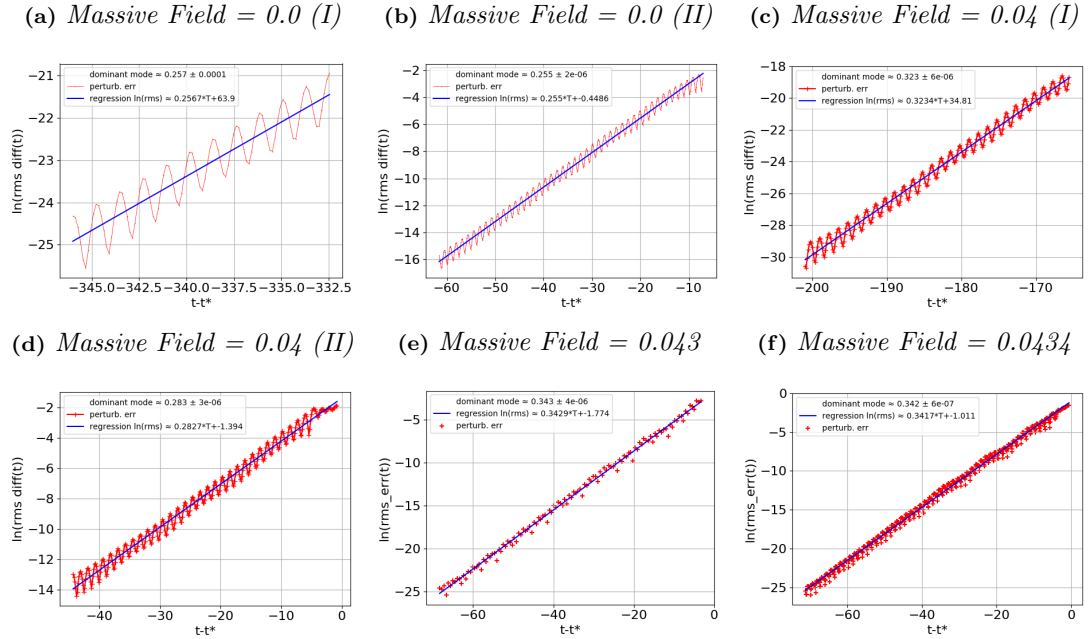


**FIG. 4:** Perturbative analyses performed on pairs of near-critical data arising from simulations near the Type I section of the collapse/dispersal boundary. Each panel represents data taken with the amplitude of the massless field fixed, while the massive field's varies. The values for  $\gamma$  reasonably match their counterparts in Table II, validating our results.

$\approx 0.32 - 0.34$  and  $\approx 0.26 - 0.28$ , which are derived from a linear time scale operant upon values of asymptotic  $t$

orders of magnitude greater than those reached in the Type II case. Considering the latter in logarithmic units

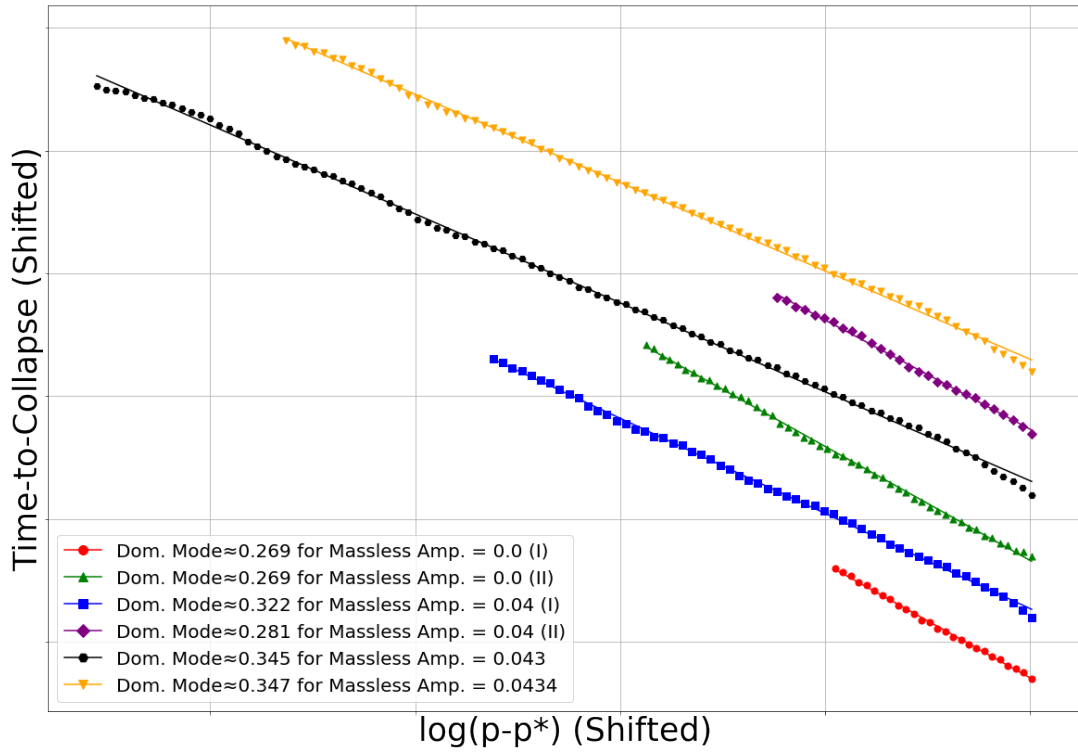


**FIG. 5:** A compilation of the linear regression analyses performed on the asymptotic times-to-collapse of the lapse along the Type I section of the dispersal/collapse boundary. Each set of points cocolored has been shifted uniformly, keeping the slope intact, so as to better present all slopes for comparison by eye. The variation in slope is readily observed.

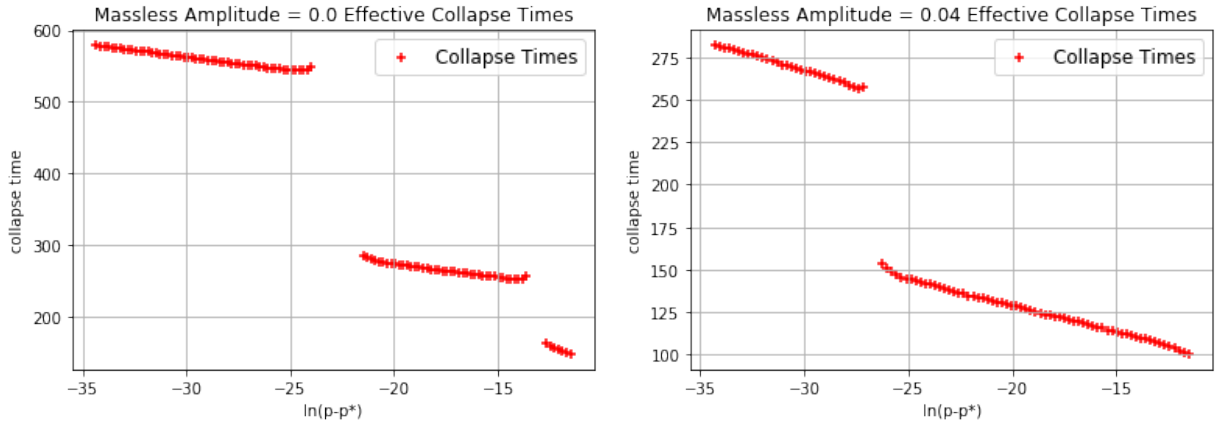


**FIG. 6:** Across the Type I section of the dispersal/collapse boundary, jumps appear the time-to-collapse of the lapse. The slopes of the two most dominant ridges of the left panel are appreciably the same, while for the right they appreciably differ. This difference is repeated in substance by their respective perturbative analyses in Figs 7 and Fig 9.

does not yield dominant modes consistent with the collapse time regressions, or even anything reasonably linear at all, wherefore it presents an improper mode of analysis, precluding equivalence with the Type II effects. For this preponderate gulf, we find the postulation of a third critical solution to be a more reasonable inference to be drawn from our results.

This deduction could furthermore explain another fea-

ture we have encountered. Between the triple point and the pure massive field regime in the phase portrait of scalar amplitudes, we find behavior a great deal more elaborate than that found by tracing out the Type II section of the boundary. This vexing situation is shown in Fig 12. The influence of the hypothetical third critical solution, whose dominant mode appears to be close in magnitude to that of the metastable star, could very

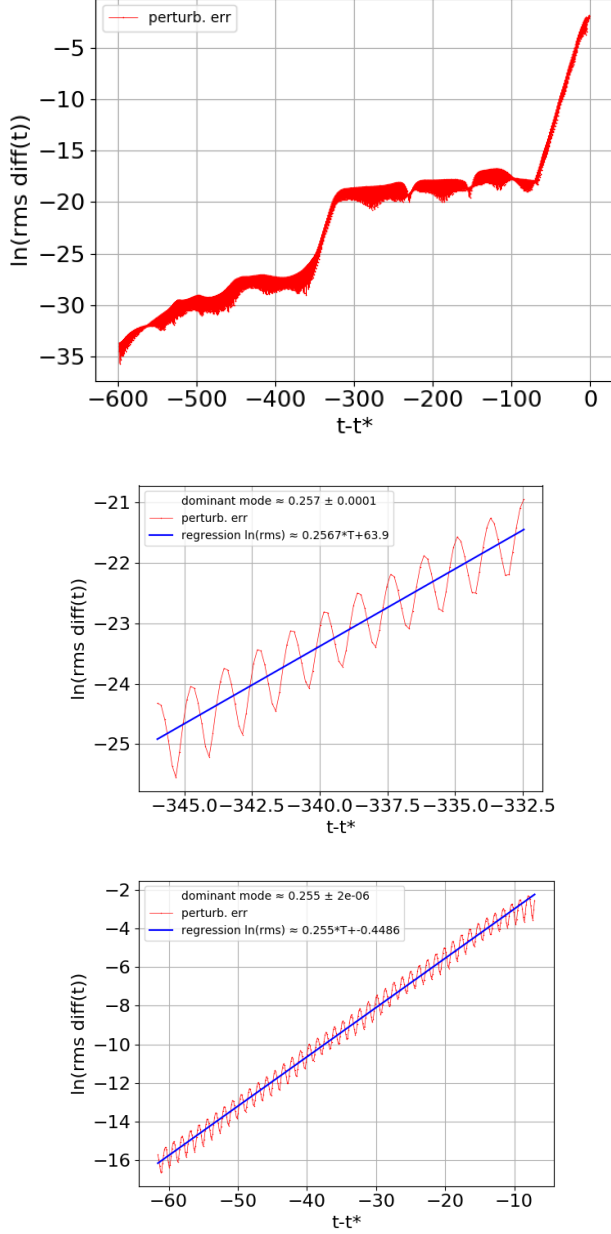


**FIG. 7:** Evolution of a perturbation away from the critical solution along the Type I section of the collapse/dispersal boundary in the case of the pure massive field. The top plot depicts the time evolution over the course of the entire simulation, and illustrates how the perturbation exhibits different regimes. The bottom two plots zoom in on the two intervals of greatest growth, whose approximately equal slopes correspond to the dominant perturbative mode for their durations.

well be responsible for this interesting phenomenon. The fact that the Choptuon is a much stronger attractor than the metastable stars and the potential third attractor, then, would explain why this effect was not seen along the Type II section of the boundary. The precision required

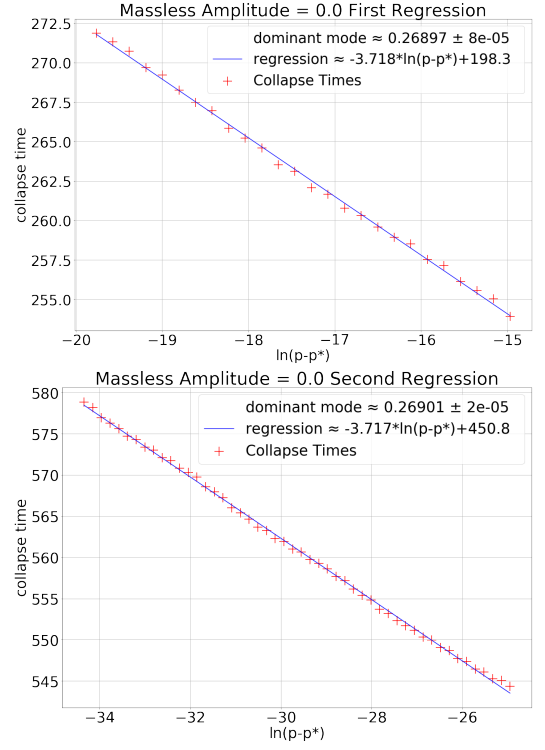


**FIG. 8:** Zoom-in regressions on the individual ridges seen in the left panel of Fig 6. The equal dominant growth modes derived from these individual ridges coincide with the modes derived from their respective intervals of perturbative evolution in Fig 7 supra.

to observe appreciable crossover between the Choptuon and the third solution's behavior – if such a crossover substantially exist at all – is far greater than that feasibly probable by our code. Moving along the Type II section of the boundary towards the triple point raises the asymptotic collapse time very slowly, likely necessitating precision well exceeding quadruple to observe values close to the lowest of the Type I case.

## V. CONCLUSION

We have put the claims advanced in our previous paper (C. Kelson-Packer and J. Belz, 2020) on more quantitative grounds by numerically investigating dominant perturbative modes across the collapse/dispersal boundary of Fig 1, employing two separate methods as cross-checks to ensure consistency. We justified our categorization for the reason of the drastically different dominant modes and time scales at play across the various sections of the dispersal/collapse boundary. Furthermore, our analysis of the varying dominant mode along the Type I section of the boundary suggests the existence of an emergent third critical solution, as we suggested following an alternative possibility considered by Gundlach et al. (C. Gundlach, T.W. Baumgarte, and D. Hilditch,



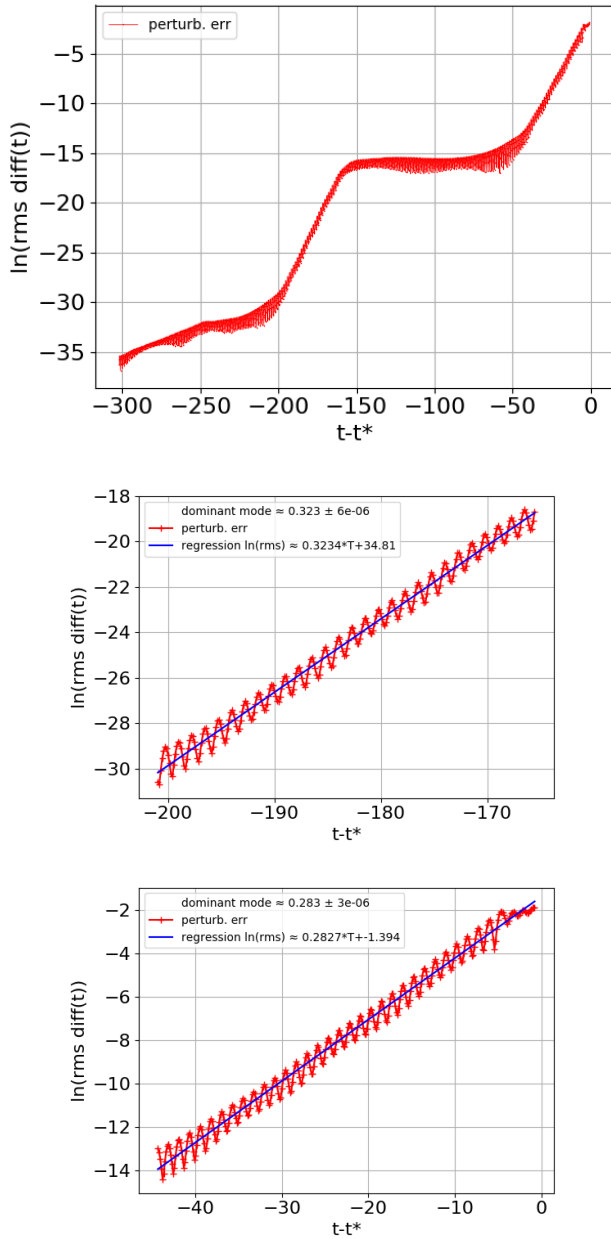


**FIG. 9:** Evolution of a perturbation away from the critical solution along the Type I section of the collapse/dispersal boundary with fixed massless field amplitude = 0.04. The top plot depicts the time evolution over the course of the entire simulation, and illustrates how the perturbation exhibits different regimes. The bottom two plots zoom in on the two intervals of greatest growth, whose differing slopes correspond to the dominant perturbative mode for their durations.

2019).

A large portion of the numerical region between the triple point and the regime of the pure massive field has proven to be numerically intractable using our current methods. While a third critical solution with influence near that of the Type I solution could explain this diffi-

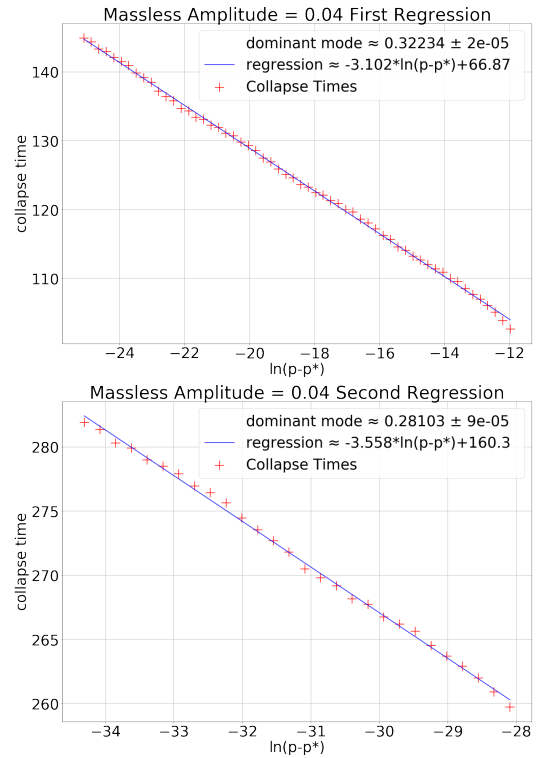


**FIG. 10:** Zoom-in regressions on the individual ridges seen in the right panel of Fig 6. The dominant growth modes derived from these individual ridges coincide with the modes derived from their respective intervals of perturbative evolution in Fig 9 supra.

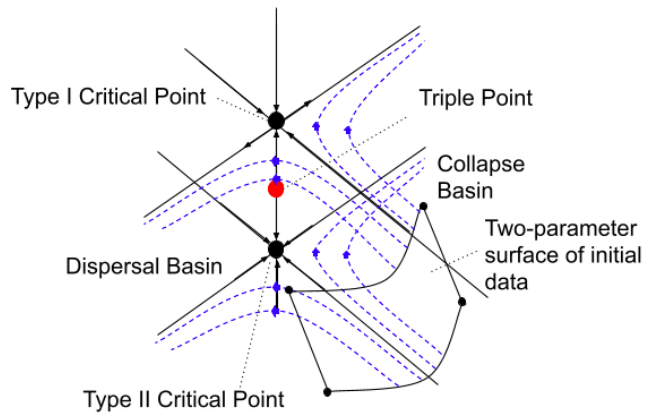


**FIG. 11:** A simplified potential picture of the dynamical system this paper investigates. The arrows suggest the local tendency of time evolution through the phase space following the most dominant growth modes. Between the interactions of the two big black dots acting in representative capacity for the most obvious parties to the system considered – the Choptuon Type II critical point and the family of metastable soliton stars corresponding to the Type I critical solution – the influence of a third factor can be detected.

cult behavior, the lack of quantitative surety leaves much unexplained absent results by a satisfactory alternative

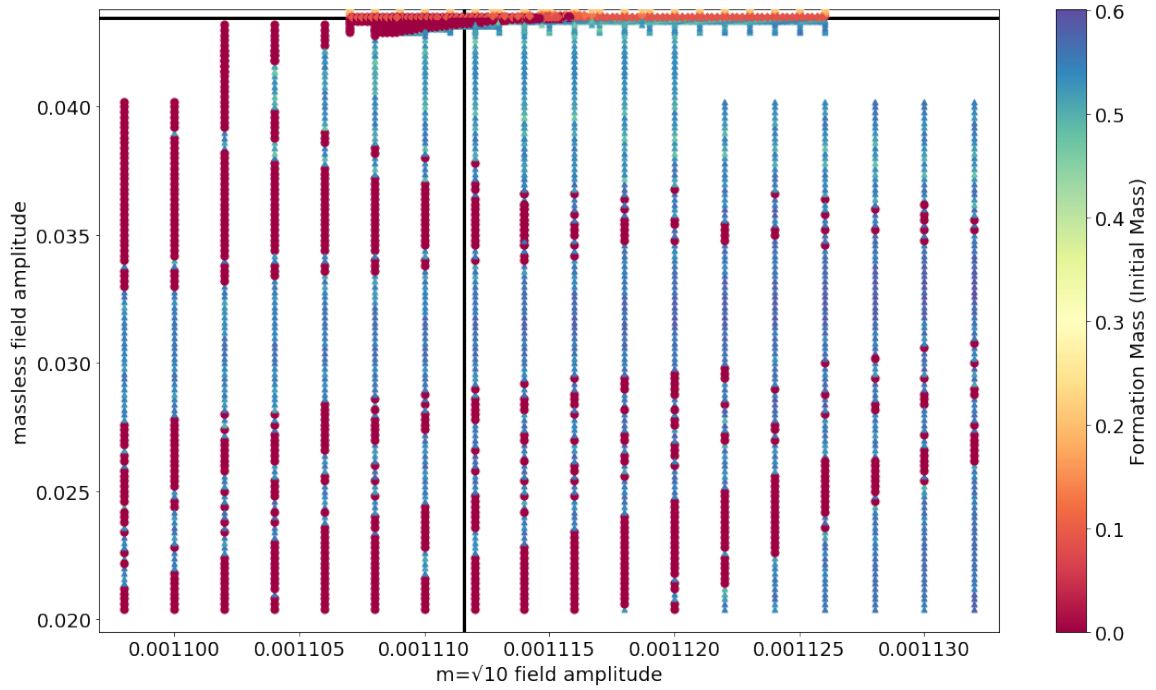


**FIG. 12:** A larger glimpse at the phase diagram seen in small part in Fig 1 supra, whose classification and depiction is the same as here. The vertical and horizontal solid lines again reflect the but-for critical amplitudes of the appropriate fields. Behavior more scurrilous than that of Fig 1 is observed, featuring “fingers” of dispersal with numerically difficult boundaries. To illustrate this more clearly, the marker size for dispersal scenarios has been made larger than those of collapsing scenarios. Qualitatively, these effects numerically persist across various levels of resolution, though we cannot rule out that some of what is shown here may be a numerical artifact. We posit that this behavior is symptomatic of the third critical solution, which becomes the primary competitor to the family of metastable soliton stars at later times in place of the Choptuon.

approach. Qualification, too, of the nature of the jumps we observe in the Type I collapse times may warrant further investigation, clarifying whether such jumps are seen close to the triple point at greater precisions, and what determines the height of the jumps and the lengths of their associated ridges. For the reason that the slopes of the ridges reflect a change in the dominant perturbative mode, we can wonder whether structures in the numerically intractable region exhibit features associated with such changes as well, since according to our hypothesis they share a common origin.

## ACKNOWLEDGMENTS

We gratefully acknowledge the technical support and computational resources of the Center for High Performance Computing at the University of Utah.

## REFERENCES

- M.W. Choptuik, Phys. Rev. Lett. **70**, 9 (1993).  
D. Christodoulou, Commun. Math. Phys. **105**, 337 (1986a).  
D. Christodoulou, Commun. Math. Phys. **106**, 587 (1986b).  
D. Christodoulou, Commun. Math. Phys. **109**, 613 (1987).  
C. Gundlach, Living Rev. Relativity **10** (2007), gr-qc/0711.4620.  
C. Gundlach, Phys.Rep **376**, 376 (2003), gr-qc/0210101.  
C. Kelson-Packer and J. Belz, Phys. Rev. D **102**, 084050 (2020), arxiv: 2008.06774.  
P.R. Brady, C.M. Chambers, and S.M.C.V. Goncalves, Phys. Rev. D **56**, R6057 (1997), gr-qc/9709014.  
C. Gundlach, T.W. Baumgarte, and D. Hilditch, Phys. Rev. D. **100**, 104010 (2019), gr-qc/1908.05971.  
T.W. Baumgarte and S.L. Shapiro, *Numerical Relativity: Solving Einstein’s Equations on the Computer* (Cambridge University Press, 2010).  
M. Alcubierre, *Introduction to 3+1 Numerical Relativity* (Oxford University Press, 2008).  
W.H. Press, S.A. Teukolsky, W.T. Vetterling, and B.P. Flannery, *Numerical Recipes: The Art of Scientific Computing* (Cambridge University Press, 2007).  
A. Stuart and A.R. Humphries, *Dynamical Systems and Numerical Analysis* (Cambridge University Press, 1998).  
S. Strogatz, *Nonlinear dynamics and Chaos* (CRC Press, 2015).  
G. Teschl, *Ordinary Differential Equations and Dynamical Systems* (American Mathematical Society, 2012).  
C. Gundlach, Phys. Rev. D **55**, 695 (1997), gr-qc/9604019.  
S. Hod and T. Piran (1996), gr-qc/9606087.  
C. Gundlach, Phys. Rev. Lett. **75**, 3214 (1995), gr-qc/9507054.  
E. Seidel and W. M. Suen, Phys. Rev. D **42**, 384 (1990a).  
E. Seidel and W. M. Suen, Phys. Rev. Lett **66**, 1659 (1990b).